Photovoltaic Performance and Morphology of Polyfluorene Blends: The Influence of Phase Separation Evolution

Rafi Shikler,* Marco Chiesa, and Richard H. Friend

Cavendish Laboratory, J. J. Thomson Avenue, Cambridge CB3 0HE, United Kingdom

Received February 26, 2006; Revised Manuscript Received June 13, 2006

ABSTRACT: We report the composition profile in blends of hole-accepting and electron-accepting polyfluorenes. During solvent evaporation to form thin (∼150 nm thickness) solid films, demixing of the polymers produces micrometer scale lateral phase separation. We show here that demixing is more complete in regions closer to the interface between the two phases. We propose that carriers transport is easier in these regions than in the bulk. We show how this affects the photovoltaic efficiency of diodes made with these blends, which show a linear dependence of efficiency on the length of the interface between the phases.

I. Introduction

There is increasing interest in electronically functional organic materials for various applications. One important application is organic photovoltaic devices made from conjugated polymers.

The photophysics of conjugated polymers is different from that of conventional inorganic semiconductors. The absorption of light generates bound electron−hole pairs,[1] in contrast to the free charge carriers which are generated in inorganic semiconductors.[2] The binding energy of this electron−hole pair, also called an exciton, is ∼0.5 eV.[3,4] To generate photocurrent, it is necessary to dissociate this strongly bounded state. The dissociation of excitons has been found to be efficient at interfaces between materials with different electron affinities and ionization potentials.[5] The difference in electron affinities and ionization potentials (or, equivalently, the offsets in the HOMO and LUMO levels) provides the energy necessary to dissociate excitons.[6,7] A configuration that maximizes the interfacial area between these materials, and therefore improves the dissociation rate of excitons, can be achieved by using polymer blends as the photoactive layer in photovoltaic devices.[5,7−10] It has been shown that the use of polymer blends increases the rate of charge transfer from the excitons, thus increasing device efficiency.[9,11] However, experimental results by Ma et al. show that the efficiency is still limited to below ∼4.5% under the so-called AM 1.5 condition.[12] A certain consensus has emerged in the literature as to the practical problems with blend-based devices and in particular with respect to morphology. Blending the polymers does lead to a large internal interface, but the p-type (hole accepting) and n-type (electron accepting) phases are far from perfectly interconnected. Hence, the conduction paths are not complete, which in turn increases recombination loss. In addition, the lack of segregation into separate p-type and n-type domains at the electrodes introduces undesired recombination pathways.

The effect of blend morphology on photovoltaic device performance is the subject of many theoretical and experimental works.

Several theoretical models have been developed for handling charge generation and transport in different blend morphologies.[13−15] Sylvester et al. had developed a general 2D hopping model for polymer-based photovoltaic devices,[16] while Watkins et al. study morphological effects using dynamical Monte Carlo simulations.[17] These works predict that device performance is optimized at an intermediate scale of phase separation, i.e., a topology that maximizes charge separation while keeping charge recombination to minimum. In both works, the best performance was obtained when there were direct percolation paths to the electrodes within each component of the blend. They both concluded that the mobility of the free carriers plays an important role in determining the quantum yield of the devices.

Extensive work has been devoted to gaining better control of the morphology of the polymer film in order to improve device performance.[11,18−21] For example, Zhang et al. show that an increase of 100% in the short-circuit current can be achieved by using chloroform mixed with chlorobenzene as a solvent.[22] In these works, morphology was controlled by modification of the device preparation parameters which affect the process of phase separation in polymer blends. These modifications were applied to parameters such as solution, concentration, substrate temperatures, spin-speed, blend composition, and solvents.

Phase separation is likely to occur when two different polymers are blended in a common solvent which is then removed, for example, during spin-casting.[23] It happens because the reduction in free energy due to the increase in entropy during mixing is not enough to compensate for the increase in enthalpy due to the mismatch of the polymer chains, and thus mixing occurs only in the presence of a solvent. During the spin-coating process or in any other process where the solvent is removed by evaporation, the polymer blend demixes and forms separate coexisting phases, with different compositions, consisting dominantly of one of the blend components. However, when the polymer blend is not given enough time to complete the phase separation (for example, fast evaporation of the solvent), an intermediate state of mixing is frozen into a solid state, with a characteristic morphology of the blend which has been reported previously.[11,21]

In this work we have focused on blends of two polyfluorene-based polymers: poly(9,9′-dioctylfluorene-*co*-bis-*N*,*N*′-(4-butylphenyl)-bis-*N*,*N*′-phenyl-1,4-phenylenediamine) [PFB] as the high mobility hole transporting polymer[24] and poly(9,9′-dioctylfluorene-*co*-benzothiadiazole) [F8BT] as a high mobility electron transport polymer. When the films are formed by spin-coating and subsequently solvent evaporation, there are two distinguishable microscopic phases: an F8BT-rich and a-PFB

* Corresponding author: e-mail rs384@cam.ac.uk; Tel 44 1223 337285; Fax 44 1223 764515.

10.1021/ma060421m CCC: $33.50
Published on Web 07/12/2006

rich phases.[25] The former is thicker than the latter. Their subsequent morphology can be described as hills and valleys. Each of these microscopic phases penetrates substantially through the film to the underlying substrate.[18]

From an optoelectronic point of view there are two distinct length scales that characterize the phase separation. The first is the length scale of the interface between the microscopic phases like the "high" and "low" phases in our system. This length scale is on the order of microns and can be inferred directly from AFM measurements. The other length scale characterizes the degree of mixing of the two polymers inside each of the microscopic phases. This length scale is of the order of nanometers. It cannot be measured using current scanning microscopic techniques but is inferred indirectly from Raman measurements or by calculating the reduction in photoluminescence efficiency measured in these phases compared to photoluminescence of the homopolymers. The nanoscale controls the process of charge transfer. The micron scale is investigated in this paper.

Blend morphology is typical studied using atomic force microscope (AFM) in contact mode,[27,26] tapping mode,[27] and lateral force mode (LFM).[28] The materials in the blend can be distinguished either by using micro-Raman spectroscopy[11] or by removal of one of the phases by a selective solvent, where applicable.[26,27,29] Near-field scanning optical microscopy (NSOM) has shown great potential in monitoring fluorescence emission with high spatial resolution (~100 nm) for polymer and fluorescent polymers.[30−32] The reviews by Stamm[33] and Krausch[34] give a through description of the relevant techniques.

Recently, Snaith et al.[19,20] reported on a linear dependence of the external quantum efficiency (EQE) of photovoltaic devices made from a similar polyfluorene polymer blend on the length of the interface separating these microscopic size phases. They postulate that this is due to the enhancement of conduction near these interfaces. The enhancement is explained by the following reasoning: Near the interface, free charges, generated by exciton dissociation, can diffuse to regions where there are preferential conduction paths; i.e., electrons/holes can diffuse to phases that are rich in electron/hole transport material, respectively. The basis for this explanation is the assumption that the mobility of the free charges depends on the composition and that these phases can be approximated to first order as having cylindrical shape. This assumption is supported by finding of Ramsdale et al.[35]

However, in that study the interface length was controlled by changing the blend ratio. Following the authors' argument that the charge transport is composition dependent, it is hard to understand why the interface length plays such an important role in these devices. Moreover, the linear dependence was found only for blend ratios in which there was a majority of one component (electron transport polymer).

All the mentioned studies successfully indicate how to improve device performance by controlling its morphology but do not give a comprehensive description of why the prescribed changes improve the performance. The reason is that although these works aimed at changing just one parameter such as blend ratio or spinning velocity, in practice they modified various parameters of the device. A good example is changing the blend ratio. Because each blend constituent has its own viscosity, changing the blend ratio leads to different device thicknesses. This can be overcome by controlling the spinning velocity to keep the thickness constant. This, in turn, affects the solvent evaporation rate and thus changes the time of the phase separation process. The same process is also being changed because the interaction between the two polymers in the blend is composition dependent, as can be seen from their phase diagram.[36]

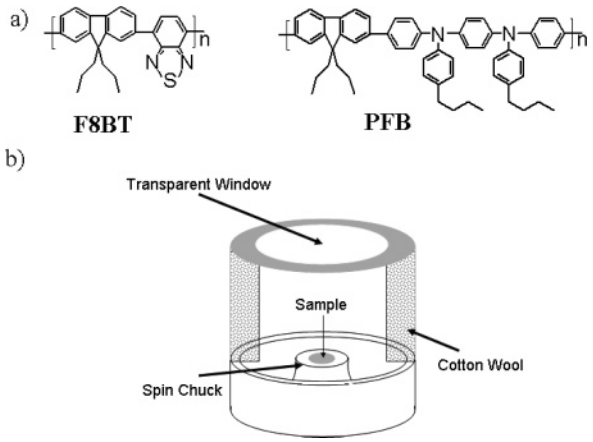

Figure 1. (a) Chemical structures of F8BT and PFB. (b) Schematic description of the controlled atmosphere.

Therefore, we have decided to follow a different approach. We have studied the relation between the blend morphology and the EQE in a controlled atmosphere experiment. A controlled atmosphere vessel enabled us to control the solvent evaporation rate. By varying the time inside the vessel, we can control the extent of the phase separation while keeping the initial phase diagram unchanged. This means that the only physical parameter that changes is the time of the phase separation process.

We show below that this method has enabled us to find the dependence of the EQE on the morphology of the phase separation. The functional form of this dependence is universal and is not affected by different blend ratios or by the excitation wavelength. In our analysis, we have adopted as a working model that the different phases as having cross-section independent of depth. We examine this model in view of our results, at the end of section IV.

II. Experimental Section

Polymer solutions were prepared by dissolving the homopolymers F8BT and PFB, whose chemical structures are shown in Figure 1a, in solutions of *p*-xylene at concentration of 15 mg/mL (1.5%). The molecular weight (M_n) of PFB was $M_n = 60\,000$, and the molecular weight of F8BT was $M_n = 62\,000$. Solution blends of F8BT:PFB were prepared by mixing different quantities of each homopolymer solution. The ratios of F8BT to PFB where 5:1, 1:1, and 1:5 by weight. We have used these blend ratios because they have measurable topographic features (blends having higher ratios do not show the valley−hill morphology for short times in controlled atmosphere). Furthermore, they represent devices were the majority of polymers is either a hole acceptor or an electron acceptor. The 1:5 and 5:1 blends have small thickness variation compared to the film thickness (~30 nm vs ~200 nm) which makes them suitable for the fabrication of photovoltaic devices. The 1:1 blend has thickness variations that are larger than half the film thickness, which makes it unsuitable for photovoltaic devices. However, the lateral size of the characteristic features in this blend is much larger than in the other blends and thus allows local probing using Raman and Kelvin probe techniques.

All the films were made in a controlled atmosphere vessel shown schematically in Figure 1b. The controlled atmosphere vessel shown in Figure 1b consists of two concentric parts: an inner chamber that holds the spin chuck and an outer part that contains solvent-soaked cotton wool. The two parts are separated by a stainless steel interface that has holes which allow the solvent to evaporate from the cotton wool to reach the inner chamber. The two chambers are

covered by a transparent cover that reduces the rate at which the solvent leaves the vessel. The polymer solution is brought into the vessel via a tube that can be sealed to prevent the escape of the solvent to the atmosphere. As the solvent evaporates from the cotton wool its partial pressure in the inner chamber increases. This in turn decreases the rate of evaporation of the solvent from the polymer solution. For example, it takes the solvent around 45 s to evaporate when casting outside the controlled atmosphere vessel compared to up to 20 min if it is cast inside the vessel.

Photovoltaic devices were prepared by spin-coating for 1 s of 60 μL of polymer blend onto a precleaned indium tin oxide-coated glass substrate, coated with a thin film of poly(ethylene dioxythiophene) doped with poly(styrenesulfuric acid) (PEDOT:PSS). The devices were then left in the controlled atmosphere vessel for durations ranging between 1 and 17 min, after which they were taken out. It was observed that the residual solvent evaporates so fast after the sample was taken outside the vessel that the morphology reached before the sample was taken out is retained. The measured thickness of the polymer layer was 220 nm. The cathode was made by evaporating 200 nm of aluminum (Al) on top of the polymer film.

Films for ultraviolet−visible (UV−vis) photoluminescence efficiency measurements and for Raman measurements were prepared on Spectrosil substrates using the same amount of polymer and the same spinning and drying time conditions. Photoluminescence efficiency measurements were carried out using an integrated sphere as in Arias et al.[11] The Raman measurements were carried out in manner similar to that of Kim et al.[36] Atomic force microscope (AFM) measurements were done both on the spectrosil and on the devices between the Al contacts. Measurements using Kelvin probe force microscope (KPFM) were done on the devices in ultrahigh vacuum (UHV).[37] The electronic performance of the devices was determined as by Snaith et al.[19]

III. Results

Figure 2 shows the morphology of a blend in a controlled atmosphere measured on the PEDOT:PSS-covered ITO samples for two different blends ratios: 1:5, 5:1 (F8BT:PFB), respectively. The images were measured using a Dimension 3100 AFM in tapping mode (Veeco Ltd.).

As can be seen in each figure, the lateral size of the typical features ("depressions" in Figure 1a−c and hills in Figure 2d−f) increases with time. This indicates that the phase separation continues to develop with time. The typical depth of the "depressions" in Figure 2a−c and the height of the hills in Figure 2d−f were in the range 20−30 nm, which is small compared to the overall film thickness (∼220 nm). We have not shown AFM measurements conducted on a 1:1 blend because, as mentioned above, the typical height difference between the two phases in the 1:1 blend was as high as 150 nm. It was observed that similar features have similar topography for the same blend at different times (see the high-resolution images in Figure 3a−c). The features also appear at the 1:1 blends ratio as seen in Figure 3d.

Figure 3a−c shows high-resolution AFM measurements of a 1:5 F8BT:PFB blend after 1, 5, and 15 min in a controlled atmosphere. It is clear that although the size of the features is different (much larger in the more developed blend) the craterlike shape is common. Figure 3d shows AFM measurement of a 1:1 F8BT:PFB blend after 15 min in a controlled atmosphere. It can be seen that inside the PFB-rich phases (the lower phases) there are the same hill shapes with a crater on top features as in Figure 3a−c.This is an indication of a second lateral scale that appears during the phase separation process due to the increase in the repulsive interaction between the blend constituents. Moreover, in the F8BT-rich phases there are features that are equivalent to the "depressions" in Figure 2a−c. The similar morphology of equivalent features indicates that they probably have similar chemical composition. We therefore conducted Raman and KPFM measurement of a 1:1 blend because the features were bigger, which is especially important for micro-Raman measurements due to low spatial resolution (just under a micron). The results are summarized in Figure 4 and Figure 5.

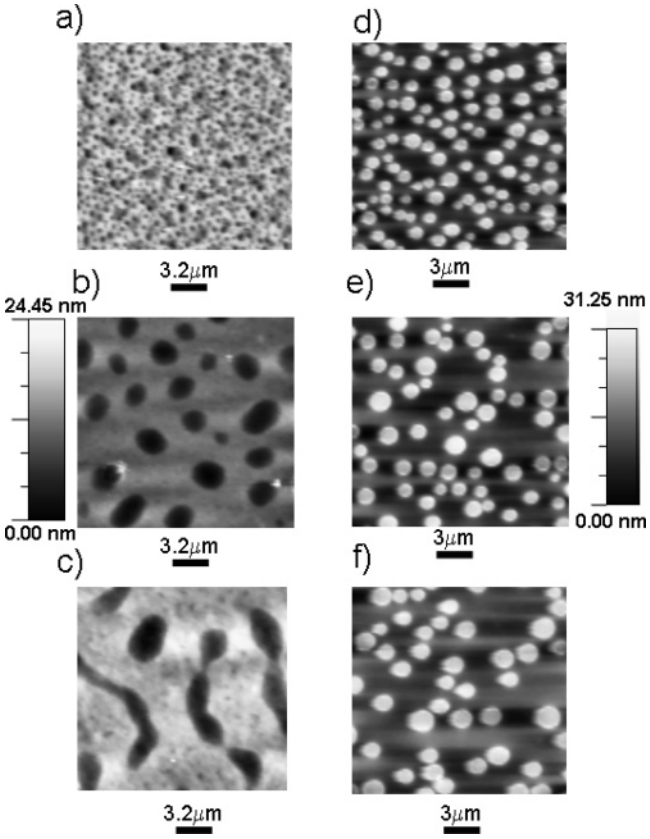

Figure 2. AFM images of samples after 1, 5, and 15 min in a controlled atmosphere. (a)−(c) and (d)−(f) are for the 5:1 and 1:5 F8BT:PFB blends, respectively. The vertical scale is the same for (a)−(c) and (d)−(f).

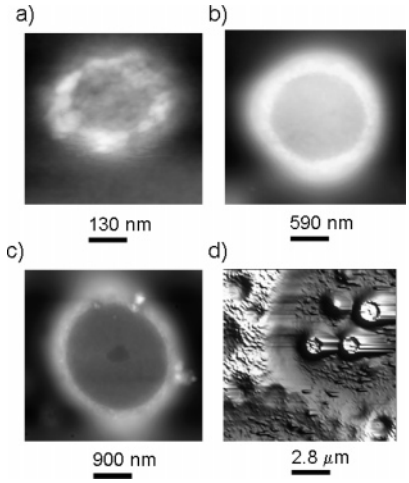

Figure 3. High-resolution AFM images of 1:5 F8BT:PFB blend after 1, 5, and 15 min in a controlled atmosphere (a)−(c), respectively. An AFM image of a 1:1 blend after 15 min shows the same features as well as features the appears in the 5:1 F8BT:PFB blend (d).

In Figure 4a an AFM image of a 1:1 blend is shown. We have indicated on this image the regions in which Raman spectroscopy was measured. These points are of the following type: (1) Regions next to the F8BT/PFB interface but on the

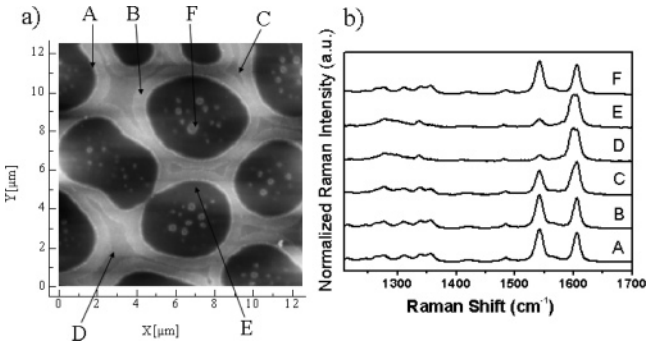

Figure 4. (a) AFM image of the 1:1 blend after 9 min in a controlled atmosphere. The brighter color is the higher phase which is the F8BT-rich phase. (b) Raman spectra of the points indicated in (a).

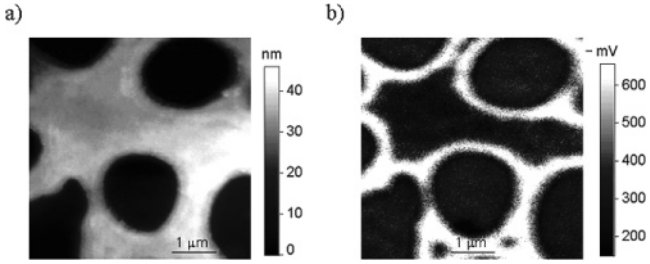

Figure 5. (a) Topography image of a 1:1 blend. (b) KPFM image taken simultaneously with the topography.

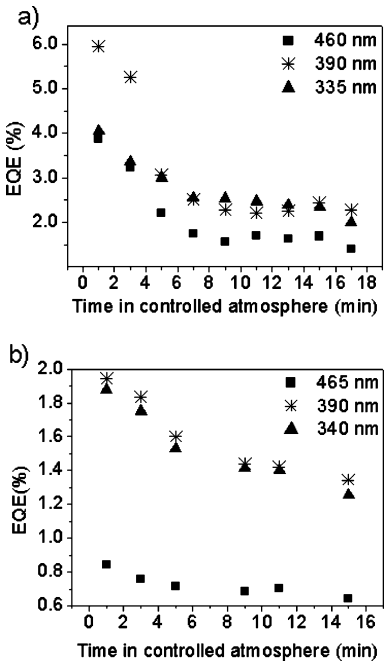

Figure 6. External quantum efficiency as a function of time in a controlled atmosphere for the absorption peaks of the homopolymers F8BT (∼460 and ∼335 nm) and PFB (∼390 nm). 5:1 F8BT:PFB blend (a); 1:5 F8BT:PFB blend (b).

F8BT side (A) and (B). These points are about 5−10 nm higher than the main F8BT phase. Points A were measured at the interface, and points B were measured at the middle of this high region. (2) Regions that are in the center of the F8BT-rich phase (C) and (D). Points C are closer to the interface than points D. (3) Regions that are in the rich PFB phase and far from any interface (E). Points on top of the F8BT-rich protrusions that have a diameter of more than 500 nm (F).

Figure 4b shows the corresponding Raman spectra. The Raman spectrum shows two strong Raman peaks at 1609 cm^{-1} (fluorene ring stretch) which is common to both F8BT and PFB and 1546 cm^{-1} (benzothiadiazole ring stretch)[38−40] which is due to the F8BT. We have calculated the ratio between the Raman cross section of F8BT and PFB following the same procedure of Kim et al.[36] and found it be $\sigma_{F8BT,1546}/\sigma_{PFB,1609} \approx \sigma_{F8BT,1609}/\sigma_{PFB,1609} \approx 1.7$ compared to 1.8 for TFB.[36] As can be seen in this figure, the feature that characterizes F8BT, i.e., the signal at 1546 cm^{-1}, is more pronounced at points A, B, and F which are either at the interface between two phases or on top of small craters. We have calculated the F8BT/PFB ratio at these points from the Raman spectra and found it to be larger than 90:10 compared to the 40:60 at points C, D, and E.

We have used the KPFM as a complementary method for measuring the chemical composition of the device. The KPFM is a variant of the AFM that can measure spatial variations of the local vacuum level of metal and semiconductors.[37] Because the local vacuum level is affected by the chemical composition,[41] this method can be used to give general information about the chemical composition profile. The main advantage of this technique is its high spatial resolution (<100 nm). KPFM measurement of a 1:1 F8BT:PFB blend is shown in Figure 5. Similar measurements of the same blend were reported before by Chiesa et al.[42]

Figure 5b shows the variation in the local vacuum level of a 1:1 F8BT:PFB blend measured under UHV conditions in the dark. This KPFM data are measured simultaneously with the topography of the film, as can be seen in Figure 5a. It is observed that the maximum change in the local vacuum level is ∼600 mV, and it takes place at the interface between the high and low phases which are the F8BT-rich and PFB-rich phases, respectively.

To understand the effect of the chemical composition on the performance of a photovoltaic device, we have calculated the quantum yield of photovoltaic devices and plotted it vs the time in a controlled atmosphere, as shown in Figure 6.

Figure 6 shows the external quantum efficiency (EQE) (calculated from the measured short circuit current, J_{SC}) of the photovoltaic devices at the peak absorption wavelengths of PFB (∼400 nm) and of F8BT (∼335 and ∼465 nm) with intensities of 0.7, 0.17, and 1.16 mW/cm^2 for the 1:5 (a) and 5:1 (b) (F8BT:PFB), respectively. The short circuit current, in this range of intensities, depends linearly on the light intensity. This implies that the EQE is independent of the light intensity. It is clear that the EQE decreases as the phase separation process evolves. The major part of the change occurs in the first 5−7 min. The changes are more pronounced in the 5:1 blend. This may be because PFB chains have higher mobility in the F8BT-rich phases than the F8BT chains in the PFB-rich phases.

The Raman measurements indicate that there is a significant difference between the chemical compositions next to the microscopic interface compared to the bulk phase. Therefore, we have replotted our results using the length of the interface separating the different phases as our independent parameter instead of the time. We have plotted the EQE at different wavelength as a function of the interface length for the two blend ratios, as can be seen in Figure 7.

For an accurate calculation of the interface length, we have used the Canny edge detection scheme.[43] To reduce the error in our calculation, we took only sample points that were between the 2%−98% percentile. Our calculation shows that the total area of each phase remains approximately the same at all times (the change in the area is about 4−5%). This excludes the area from being a good parameter for characterizing the evolution of the phase separation. The constant area of each phase also

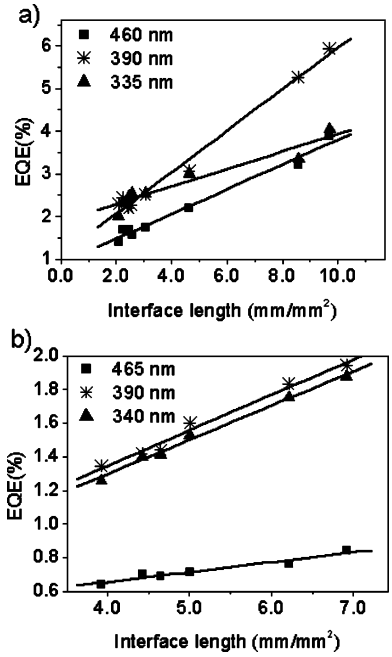

Figure 7. External quantum efficiency as a function of interface length for the excitation at the wavelength of the peaks of the absorption spectra of the homopolymers F8BT and PFB together with a linear fit. (a) 5:1 F8BT:PFB blend; (b) 1:5 F8BT:PFB blend.

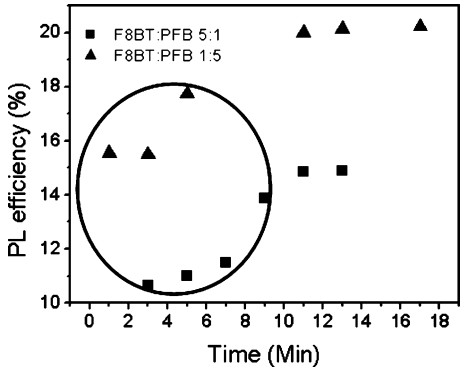

Figure 8. Photoluminescence efficiency as a function of time in a saturated atmosphere for 1:5 and 5:1 F8BT:PFB blends. The circle encompasses the points that are relevant to the fabricated device. (triangles for 1:5 and squares for 5:1 (F8BT/PFB), respectively).

Table 1. Values of the EQE for the Limiting Case of Zero Interface Length vs Blend Ratios 5:1 and 1:5 F8BT:PFB, Respectively

excitation wavelength (nm)	EQE at zero interface length for 5:1 (%)	EQE at zero interface length for 1:5 (%)
335	0.91	0.5
390	1.98	0.52
460	1.1	0.43

indicates that there is no obvious vertical phase separation process. However, for both blend ratios, the interface length decreases with time.

The interface length is measured in mm/mm^2 because we have calculated the length of the interface per unit area of AFM image. We have fitted the EQE to the following equation: EQE $= C \times$ interface length $+$ EQE$_0$, where the constant C is the slope of the linear fit and EQE$_0$ is the extrapolated value of the EQE in the limit of zero interface length. The extrapolated EQE values for the limiting case of zero interface length are summarized in Table 1.

Photoluminescence efficiencies measured for thin films of the phase-separated blends are shown in Figure 8. The measured PL efficiency of the polymer blend films is small in comparison to the PL efficiency of films made from the homopolymers. The values, as measured in this work, for the homopolymers are 55% and 39% for F8BT and PFB, respectively, compared to less than 20% for the blends. The quenching of the PL implies efficient charge transfer in the blend films. Figure 8 shows that the PL efficiency increases with time. This indicates that the efficiency of charge transfer decreases with the development of the phase separation. However, the measured values are still small compared to the homopolymer values even for the well-developed films. The maximum change in the PL efficiency quenching between two films of the same blend for different times in the controlled atmosphere vessel is $\Delta PL/(PL(t = t_1)) = |[PL(t = t_2) - PL(t = t_1)]/(PL(t = t_1))| \approx 33\%$; $t_2 > t_1$.

IV. Discussion

The most significant finding of this research is the composition profile found in these blends. This can be deduced from the Raman measurements (see Figure 4), which show that at the microscopic interface there is a large concentration of F8BT (>90%). It was also shown by the change in the local vacuum level at the interface, which is around 600 mV (see Figure 5). This change is smaller than the difference between the position of the middle of the HOMO−LUMO gap of the homopolymers, ∼1 V. However, the KPFM has finite resolution (∼50 nm) which enables only the measurement of average values on this length scale. We can therefore define the average local vacuum level by summing the local vacuum levels of the homopolymer with weights that are proportional to composition profile, which we assume to be homogeneous on length scales below 50 nm.

Calculating the F8BT:PFB ratio at the PFB side of the interface from the Raman measurement to be ∼60:40% and using the above reasoning, the expected difference is 500 ± 50 mV. This is in agreement with measured potential profile. The error is due to error in the composition evaluation and also due to the unknown contributions from the ITO:PEDOT interface.

We can therefore conclude that F8BT is trapped at the microscopic interface. Moreover, our findings show that in the middle of the presumably F8BT-rich phase the chemical composition is the same as in the PFB-rich phase. These findings extend the common framework of phase separation, namely spinodal decomposition or nucleation, where the former predicts and increase in size and purity of the separated phases with time and the latter predicts pure phases whose size grows with time. The difference between the investigated system and those commonly reported in the literature is the different miscibility of the homopolymers in the solution. Kim et al.[36] showed that F8BT becomes immiscible in *p*-xylene when its concentration exceeds 3.8% compared to around 90% for PFB. This large asymmetry indicates a different dynamics of the phase-separating blends which leads to the trapping of the less miscible polymer at the interface.

During the process of phase separation each homopolymer is driven toward the phase where it has high concentration, F8BT diffuses from the PFB-rich phase to the F8BT-rich phase, and the opposite holds for PFB. As a result, there is a high concentration of each of the homopolymers next to the interface on their relative sides. Therefore, when the F8BT concentration exceeds a value of ∼3.8%, the F8BT is trapped at the interface. Moreover, it creates a barrier that prevents the PFB in the rich F8BT phase to diffuse to the other side. As a result, we have an interface that grows both into the PFB-rich phase and into the F8BT-rich phase. Our findings are in good accordance with findings of simulation of phase separation when one of the

constituents forms a glassy phase.[44−47] This hypothesis is consistent with the increase in poly(9,9′-dioctylfluorene) (PFO) fluorescence at the domain boundaries in NSOM experiments in PFO:F8BT blends studied by Chappel et al.[48]

We have also compared the relevant length scales in the Raman and KPFM measurements. The interface width as seen in the topography and KPFM is on the order of 200 nm, and in the Raman measurements the observed interface width, as deduced from the topography, is on the order of 750 nm−1 μm.

Similar behavior is observed in the 5:1 blend. On the basis of the above findings we deduced that the chemical structure near the interface is probably similar for the same blend ratio at all times. The changes are in the spatial extent of this interface. If we add to this conclusion that it is the F8BT that precipitated first from the solution, we can conclude that for all the blends there is a peak in the concentration of F8BT at the microscopic interface.

Because the fraction of the homopolymers (predominantly F8BT) is high at the microscopic interfaces, the density of traps, i.e., the other polymer that can lower the conduction, is small. Therefore, we can assume that there is enhanced conduction, which is due to enhancement either of the mobility or of the free charges lifetime near these interfaces compared to the bulk of the film. The free charges that are created from exciton dissociation next to the microscopic interface can diffuse to the interface where there is preferential conductance for electrons. These electrons have higher probability to reach the cathode and be collected than those which are created in the bulk of the film. This finding is supported by the work of Snaith et al.[19]

Before we follow with this approach we need to verify that it is indeed charge transport and not charge transfer that controls the behavior of the EQE. This is studied below.

Figure 6 shows that the EQE of the devices decreases with the evolution of the phase separation. The EQE goes down from 6% to 2% for the 5:1 blend at 460 nm and from 2% to 1.2% for the 1:5 blend at the same wavelength. Since the process of converting light to electricity consists of two major parts, charge transfer and charge transport, it is logical to investigate the effect each has on the EQE. Charge transport cannot be measured directly; hence, we checked whether charge transfer could explain the strong dependence of the EQE on the device morphology. Charge transfer can be deduced from photoluminescence efficiency measurement. The degree of charge generation is inferred from the degree of photoluminescence quenching in the blend with respect to the homopolymer. Therefore, photoluminescence efficiency can be used to study the morphology dependence of the charge-transfer efficiency.

We have seen above that the PL efficiency increases with the evolution of the phase separation process. This implies that the charge-transfer process becomes less efficient and should therefore lead to a reduction in the EQE of up to 33%. However, correlation between PL efficiency and EQE measurements has to be done for the same morphology. We have compared the AFM images of a phase-separated blend, spin-cast on a spectrosil substrate, to those of one cast on PEDOT:PSS covered ITO. The typical size of the topographic features measured on the PEDOT:PSS-covered ITO samples was around half the size of those that were measured on spectrosils for samples that spent the same time in the controlled atmosphere vessel. This difference is because the phase separation process is influenced by the substrate surface (see Puri[49] and references therein). Therefore, the relevant times are those below 9 min (as indicated by the circle in Figure 8). Recalculating the changes in the PL efficiency measured on the samples in this time region shows that the maximum change in PL efficiency is less than 17% for the 1:5 F8BT:PFB blend and less than 25% for the 5:1 F8BT:PFB blend. In comparison, the maximum changes in the EQE were 70% and 400% for the 1:5 and 5:1 blends, respectively.

This indicates that changes in the PL efficiency are not sufficient to explain the reduction in the EQE. Therefore, the limiting factor for the EQE is charge transport.

Therefore, we tested the assumption that the high mobility of charge carriers next to the microscopic interface due to purer polymers is the factor that controls the EQE. According to this assumption, the EQE is expected to have a linear dependence on the interface length because the number of carriers that can reach the interface is proportional to its length.

Figure 7 shows that in general the EQE depends linearly on the length of the interface between the microscopic phases (one exception is the EQE of the 5:1 F8BT:PFB blend at excitation wavelength of 335 nm). This justifies the choice of the interface length as a parameter for characterizing the morphology in the context of EQE measurements.

We can see that in the 5:1 F8BT:PFB blend the EQE is larger for the minority excitation (the EQE at 390 nm) as expected because charge conduction is limited by the minority phase ability to conduct charges.

In the 1:5 F8BT:PFB blend the EQE is similar for the majority and minority constituents. The discrepancy in the 335 nm excitation can be explained by the asymmetry of the illumination. The illumination is from the ITO side, i.e., the anode side; hence, there is a preference for hole conduction. This obviously changes the relative contributions of the two homopolymers in favor of the PFB.

It is important to notice that if the charge transport was the only mechanism that contributed to the EQE, the extrapolated value of EQE for the limiting case of zero interface length would have been zero.

It is evident from Table 1 that the EQE does not go to zero with zero interface length. This is an indication that there is an additional mechanism that contributes to the current other than the conduction along the interface. Moreover, the extrapolated value for the EQE at zero interface length is almost the same for all wavelengths excitations at a specific blend ratio (one exception is the 390 nm at 1:5 F8BT:PFB blend). A possible explanation for the first observation is the presence of a wetting layer of PFB on the substrate, as reported by Kim et al.[36] The interface of the wetting layer and the blend can be regarded as a bilayer configuration, which contributes to the current regardless of the interface length. An additional indication for the validity of this assumption is that the EQE_0 is higher for the 5:1 (F8BT:PFB) blend compared to the 1:5 blend. This is because the PFB wetting layer contributes most to charge transfer if it has a large interface with F8BT. This is more probable for the 5:1 blend than the 1:5 blend. An alternative explanation is that this current is just due to the bulk contribution because, as we reported above, the bulk of the microscopic phases is not pure; therefore, it contributes to charge transfer as well as to charge transport, as can be seen by the PL quenching in Figure 8. The nonzero value of EQE_0 shows that the depth independent cross-section description of the different phases is only a first-order approximation. However, the small value of EQE_0 indicates that it is a good approximation.

V. Conclusions

In this paper we have investigated the process of phase separation in polyfluorene blends (F8BT:PFB) and the depen-

dence of the EQE of photovoltaic devices on this process. We show by measuring the composition profile of the homopolymers at the interface that the simple picture of spinodal decomposition does not apply to our system. Our measurements indicate that the homopolymers (predominantly F8BT) are trapped at the interface. We also show that the composition profile next to the interface is nearly time independent by showing that the morphological features have the same shape at all times.

We have studied the dependence of the EQE on the phase separation process and show that it is limited by charge transport and not by charge transfer. On the basis of our findings regarding the chemical composition, we have assumed that the homopolymers that are trapped at the interface create preferable conduction channels for electrons/holes in the F8BT/PFB side, respectively.

We have checked this assumption by parametrizing the microscopic morphology of the device using the microscopic interface length as a parameter. We have found a linear dependence of the EQE on this parameter, thus confirming our model.

We have also studied the extrapolated EQE value for zero interface length and show that it is not zero. This finding indicates that although the EQE is limited by charge transport at the microscopic interfaces there are nonnegligible contributions either from the bulk of the film or from wetting layers at the polymer−contact interface.

Future work should focus on directly measuring the chemical composition at the interface using different methods. We would also like to measure phase separation on smaller time scales. The EQE should also be measured locally for better understanding of electronic process at the interface.

Acknowledgment. This work was supported by the European Commission (NAIMO NMP4-CT-2004-500355).

References and Notes

(1) Pope, M. S.; Swenberg, C. E. *Electronic Processes in Organic Crystals;* Oxford University Press: Oxford, 1982.
(2) Bube, R. H. *Photoelectronic Properties of Semiconductors;* Cambridge University Press: Cambridge, 1989.
(3) Marks, R. N.; Halls, J. J. M.; Bradley, D. D. C.; Friend, R. H.; Holmes, A. B. *J. Phys.: Condens. Matter* **1994**, *6*, 1379.
(4) Brédas, J.; Cornil, J.; Heeger, A. J. *Adv. Mater.* **1996**, *8*, 447.
(5) Tang, C.; VanSlyke, S. *Appl. Phys. Lett.* **1987**, *51*, 913.
(6) Halls, J. J. M.; Walsh, C. A.; Greenham, N. C.; Marseglia, E.; Friend, R. H.; Moratti, S. C.; Holmes, A. B. *Nature (London)* **1995**, *376*, 498.
(7) Yu, G.; Gao, J.; Hummelen, J.; Wudl, F.; Heeger, A. *Science* **1995**, *270*, 1789.
(8) Kim, J.; Granstrom, M.; Friend, R. H.; N. Johansson, W. S.; Daik, R.; Feast, W.; Cacialli, F. *J. Appl. Phys.* **1998**, *84*, 6859.
(9) Brabec, C.; Sariciftci, N.; Hummelen, J. *Adv. Funct. Mater.* **2001**, *11*, 15.
(10) Pacios, R.; Bradley, D. D. C. *Synth. Met.*. **2002**, *127*, 261.
(11) Arias, A. C.; MacKenzie, J. D.; Stevenson, R.; Halls, J. M.; Inbasekaran, M.; Woo, P. E.; Richards, D.; Friend, R. H. *Macromolecules* **2001**, *34*, 6005.
(12) Ma, W.; Yang, C.; Gong, X.; Lee, K.; Heeger, A. J. *Adv. Funct. Mater.* **2005**, *15*, 1617.
(13) Gregg, B. A.; Hanna, M. C. *J. Appl. Phys.* **2003**, *93*, 3605.
(14) Gregg, B. A. *J. Phys. Chem. B* **2003**, *107*, 4688.
(15) Malliaras, G. G.; Salem, J. R.; Brock, P. J. Scott, J. C. *J. Appl. Phys.* **1998**, *84*, 1583.
(16) Sylvester-Hvid, K. O.; Rettrup, S.; Ratner, M. A. *J. Phys. Chem. B* **2004**, *108*, 4296.
(17) Watkins, P. K.; Walker, A. B.; Verschoor, G. L. B. *Nano Lett.* **2005**, *5*, 1814.
(18) Halls, J. M.; Arias, A. C.; Mackenzie, J. D.; Wu, W.; Inbasekaran, M.; Woo, E. P.; Friend, R. H. *Adv. Mater.* **2000**, *12*, 498.
(19) Snaith, H. J.; Arias, A. C.; Morteani, A. C.; Silva, C.; Friend, R. H. *Nano Lett.* **2002**, *2*, 1353.
(20) Snaith, H. J.; Friend, R. H. *This Solid Films* **2004**, *451*−*452*, 567.
(21) Moons, E. *J. Phys.: Condens. Matter* **2002**, *14*, 12235.
(22) . Zhang, F.; Jesperson, K. G.; Björström, C.; Svensson, M.; Andersson, M. R.; Sundström, V.; Magnusson, K.; Moons, E.; Yartsev, A.; Inganäs O. *Adv. Funct. Mater.* **2006**, *16*, 667.
(23) Bates, F. S. *Scienc*e **1991**, *251*, 898.
(24) Redecker, M.; Bradley, D. D. C.; Inbasekaran, M.; Wu, W.; Woo, E. *Adv. Mater.* **1999**, *11*, 241.
(25) Stevenson, R.; Arias, A.; Ramsdale, C.; MacKenzie, J.; Richards, D. *Appl. Phys. Lett.* **2001**, *79*, 2178.
(26) Walheim, S.; Ramstein, M.; Steiner, U. *Langmuir* **1999**, *15*, 4828.
(27) Walheim, S.; Böltau, M.; Mlynek, J.; Krausch, J.; Steiner, U. *Macromolecules* **1997**, *30*, 4995.
(28) Cyganik, P.; Budkowski, A.; Raczkowaska, J.; Postawa, Z. *Surf. Sci.* **2002**, *507*−*510*, 700.
(29) Affrossman, S.; Henn, G.; O'Neill, S. A.; Pethrick, R. A.; Stamm, M. *Macromolecules* **1996**, *29*, 5010.
(30) Betzig, E.; Trautmann, J. K. *Science* **1992**, *257*, 189.
(31) Aoki, H.; Sakurai, Y.; Its, S.; Nakagawa, T. *J. Phys. Chem. B* **1999**, *103*, 10553.
(32) Stevenson, R.; Milner, R. G.; Richards, D.; Arias, A. C.; MacKenzie, J. D.; Halls, J. J. M.; Friend, R. H.; Kang, D. J.; Balmire, M. *J. Microsc.* **2001**, *202*, 433.
(33) Stamm, M. *Adv. Polym. Sci.* **1992**, *100*, 357.
(34) Krausch, G. *Mater. Sci. Eng.* **1995**, *R14*, 1.
(35) Ramsdale, C. M.; Bache, I. C.; MacKenzie, J.; Thomas, D. S.; Arias, A. C.; Friend, R. H. *Physica E* **2002**, *14*, 268.
(36) Kim, J. S.; Ho, P. K. H.; Murphy, C. E.; Friend, R. H. *Macromolecules* **2004**, *37*, 2861.
(37) Nonnenmacher, J.; Wolter, O.; Greschner, J.; Kassing, R. *J. Vac. Sci. Technol. B* **1991**, *9*, 1358.
(38) Kim, J. S.; Ho, P. K. H.; Murphy, C. E.; Baynes, N.; Friend, R. H. *Adv. Mater.* **2002**, *14*, 206.
(39) Ariu, M.; Lidzey, D. G.; Bradley, D. D. C. *Synth. Met.* **2000**, *111*−*112*, 607.
(40) Colthup, N. B.; Daly, L. H.; Wiberley, S. E. *Introduction to Infrared and Raman Spectroscopy*, 3rd ed.; Academic Press: San Diego, 1990.
(41) Becker, J. A. *Rev. Mod. Phys.* **1935**, *7*, 95.
(42) Chiesa, M.; Bürgi, L.; Kim, J. S.; Shikler, R.; Friend, R. H.; Sirringhaus, H. *Nano Lett.* **2005**, *4*, 559.
(43) Canny, J. *IEEE Trans. PAMI* **1986**, *8*, 679.
(44) Sappelt, D.; Jackle, J. *Europhys. Lett.* **1997**, *37*, 13.
(45) Jackle, J.; Sappelt, D. *Polymer* **1998**, *39*, 5253.
(46) Sharma, J.; Puri, S. *Phys. Rev. E* **2001**, *64*, 21513.
(47) Sappelt, D.; Jackle, J. *Physica A* **1997**, *240*, 453.
(48) Chappell, J.; Lidzey, D. G.; Jukes, P. C.; Higgins, A. M.; Thompson, R. L.; O'Connor, S.; Grizzi, I.; Fletcher, R.; O'Brien, J.; Geoghegan, M.; Jones, R. A. L. *Nat. Mater.* **2003**, *2*, 616.
(49) Puri, S.; Frisch, H. L. *J. Phys.: Condens. Matter* **1997**, *9*, 2109.

MA060421M